RC25492 (MRL1408-004) August 27, 2014
Chemistry

IBM Research Report

Expansion and Dynamic Stability of Gases between Two Amorphous Silica Particles in Aqueous Solution

A. Bojovschi, S. Moore, S. A. Chen, P. Rogers
IBM Research Division
204 Lygon Street
Carlton, Victoria 3053
Australia

Research Division
Almaden – Austin – Beijing – Cambridge – Dublin - Haifa – India – Melbourne - T.J. Watson – Tokyo - Zurich

Expansion and dynamic stability of gases between two amorphous silica particles in aqueous solution

A. Bojovschi,* S. Moore, S. A. Chen, P. Rogers

IBM Research – Australia, 204 Lygon Street, Carlton, Victoria 3053, Australia

Abstract. The present work reports on the dynamics of gaseous nano-bubbles of CO_2, and air (N_2 and O_2) confined between two deprotonated amorphous silica surfaces. The study uses molecular dynamics simulation. The results show that nano-bubbles of these gases can be stabilized between two amorphous silica surfaces. The stability is evident from the volumetric data and density analysis. We also propose that the stability of the nano-bubbles is linked to the diffusion of gas molecules in and out of the bubbles. The mean values of contact angle of CO_2 and air nano-bubbles confined by amorphous silica were found to be on average between 17 and 27 degrees. The volumetric expansion of dense nano-bubbles to equilibrium follows a sigmoid. The data show that this leads to a decrease in gas density in the nano-bubble following a first order exponential decay. The results are in agreement with wettability measurements and experimental studies that investigated the presence of nano-bubbles between amorphous silica surfaces.

*Author to whom correspondence should be addressed: Electronic mail: alexe.bojovschi@au1.ibm.com

I. INTRODUCTION

Structural dynamics of gases such as N_2, O_2 and CO_2 at the interface between mineral surfaces play a key role in flotation, cleaning and CO_2 sequestration technologies. Silica (SiO_2), accounting for about 28% of the earth, is the most common mineral and a fundamental constituent of glass. Silica exhibits a tetrahedral network structure in which silicon atoms are the centers of the tetrahedra with oxygen atoms working as bridges between them. The characteristics of silica surfaces were shown to be of importance in production and functionalization of modern materials such as reinforced polymer matrix composites, oxide semi-conductors and ultrahigh nano-porous structures.[1-5] Silica in colloidal form[6] has aided the development of traditional application in the coating, food and paper industries,[7,8] and more recently in the biomedical industry.[9,10] These have driven a large amount of theoretical, experimental and computational studies. Experimental studies of silica surfaces generally encompass Raman spectroscopy, thermogravimetric analysis (TGA), atomic force microscopy (AFM), Nuclear Magnetic Resonance (NMR) and Fourier transform infrared (FT-IR) spectroscopy techniques.[11-22] The importance of studying not only the bulk properties of silica but also the surface properties was clearly mentioned in a review by Pantano.[23] Theoretical and computational methods that could predict the properties of silica were developed, covering large lengths and time scales. Computational methods include various types of *ab initio* type calculations.[12,13,24-29] These were extended using methods that allow time scales of orders 10^3 to 10^5 longer than quantum mechanical calculations. Examples of such methods are Monte Carlo (MC), Molecular Dynamics (MD) and Brownian Dynamics (BD) simulations. Mesoscale methods including MC and BD[30-35] were used to achieve longer time scales at the expense of losing the atomistic level details. Molecular simulation of the silica surface and

interfaces as well as their interaction with water or small molecules was reported in numerous studies.[37-44]

The use of dehydroxylated/deprotonated and artificially hydroxylated/protonated amorphous silica surfaces were investigated.[45-48] Using estimates from absorption potential and surface diffusion of three weakly bound adsorbates, Stallons and Iglesia[46] evaluated two kinds of hydroxylated surfaces. The study showed that relaxed, compared to un-relaxed, surfaces show greater heterogeneity and wider distribution of adsorption energy. MD simulations carried out by Leed and Pantano[47] were used to assess the adsorption of water on deprotonated and artificially hydroxylated surfaces. The large majority of work involved hydroxylated silica surfaces, where the hydroxyl groups are responsible for the water adsorption. Results obtained by Bakaev and Steele, that used deprotonated silica surfaces, indicated that the surface defects are also responsible for attractive forces on polar molecules.[48] These defects include 3-coordinated silicon and nonbridged oxygen (NBO) which contribute to the strong electrostatic field responsible for attractive forces. The study indicated that the irregularities of the amorphous silica surfaces and its roughness define its affinity for polar molecules. Quantum mechanical studies revealed that the structure of water near the silica surface is different from that in the bulk.[49] The role of water induced damage of the self assembled monolayers of alkylsilane molecules on amorphous silica were also addressed by Lane et al.[50]

Large number of MD studies have provided insights on the static and dynamics aspects of amorphous and crystalline silica.[51-67] Multiscale approaches were also used to cover large time and length scales.[68-71] Computational methods were employed to study the behavior of liquids confined between substrates. These included the wetting behavior[72-76] and the range of different forces resulting from different wettability conditions.[77] The role

of surface topography and temperature were shown to influence the substrate-fluid interaction strength.[78-79] The presence of nano-bubbles on and between hydrophobic particles were studied using experimental and computational coarse grain methods.[80] These were driven by numerous questions regarding the role and existence of these nano-bubbles. Some of the inquiries were related to their spontaneous appearance at the interface between a liquid and a hydrophobic surface[81-83] and their role on the liquid slip and drag at the interface and the long range attraction forces.[84-87] The presence of nano-bubbles were detected using techniques such as neutron reflectometry,[88] rapid cryofixation,[89] X-ray reflectivity measurements,[90] optical spectroscopy,[91] optical microscopy[92] and tapping mode atomic force microscopy.[81] The recent indication that nano-bubbles also play a role in the attraction of hydrophilic surfaces[93] suggests a new avenue to be explored with the available knowledge obtained from their studies in the proximity of hydrophobic surfaces.

Although the interactions between silica surfaces have been addressed in a number of studies, there is still uncertainty regarding their interaction in solution. The majority of studies that approach force curves did not notice the presence of an adhesion force between silica particles.[94-96] Studies indicated that the adhesion between silica surfaces in water occurred only after the surfaces stay in contact for a long time.[94] Other studies showed that the strength of adhesion between silica surfaces decreased after several days in water.[95] Chapel, reported that silica-silica adhesion disappeared after few minutes in water with a concentration of 0.1 M NaCl at a pH of 5.5.[96] The role of salt concentration on the adhesion of silica-silica surfaces provided contradictory results. Results obtained by Yaminsky et al.[95] and Megher[97] indicated an increase in adhesion while Vakarelski et al and Fielden found a decrease in adhesion with salt concentration.[98] Furthermore the results obtained by Freitas and Sharman[99] indicated no relationship between the

concentration of electrolyte and the adhesion value between two silica surfaces. The elusive forces between silica particles that led to these different results were shown to be due to the presence or absence of nano-bubles[93]. The authors pointed out that dehydroxylated silica surfaces may have been responsible for the cavities/bubbles. However, cavities/bubbles would need to be considered in the analysis of measured force curves between silica surfaces as they might never be totally absent.

To the best of our knowledge, atomic level simulation of three-phase systems consisting of a solid silica surface, nano-sized gas phase and liquid solvent has not been previously undertaken. In this study, we investigate using atomistic simulation the dynamics and stability of CO_2 and air nano-bubbles between silica surfaces in water. This work is a first step towards deciphering, the role played by nano-bubbles in increasing or decreasing the interaction between silica surfaces from an atomic level.

II. METHODS

A. Modeling air and CO_2 between silica particles in solution

Understanding the dynamics of gas bubbles in solution requires the modeling of a fully solvated atomistic structure. In this work, spherical volumes of CO_2 and air (N_2 and O_2) were placed between two amorphous silica surfaces and were fully solvated (Fig. 1). The air mixture consisted of 80% N_2 and 20% O_2. Noble gases of Ar and Ne, and compounds of CO_2 and CH_4 were not considered in this mixture due to their inherently low concentration. A summary of the investigated systems with their gas phases including the number of atoms and molecules is presented in Table 1. The three dimensions in the Cartesian system of the two identical, dehydroxylated amorphous silica particles are x = 17.1860 nm, y = 17.1427 nm and z = 13.0318 nm. The initial state of the systems corresponded to a dense gas phase with all molecules situated in a sphere of 3 nm radius.

The gas sphere was situated at 0.3 nm away from the center of the lower silica layer. The initial density of air was 0.052 a.u./Å^3 and of CO_2 was 0.109 a.u./Å^3. The solvent used in both systems (Fig. 1) is water.

Our own routines programmed in bash, Visual Molecular Dynamics (VMD)[100] and ImageJ[101] were used to: (a) build the simulated systems, (b) check for steric clashes, (c) analyze the simulation trajectory, and (d) perform structural analyses. The amorphous silica layers were generated using the InorganicBuilder within VMD. The tcl scripting interface in VMD was used to generate all the other components of the simulated systems. The representation and coloring method used for presenting atomic structure of CO_2, N_2, O_2 and SiO_2 is the Corey, Pauling and Koltun (CPK) space filling molecular model.[102] The CPK method renders the atoms as spheres with the size determined by the van der Waals (vdW) radius. The surface rendering method, as implemented in VMD., was also used. The atom colours are depicted by the accepted color conventions for carbon (cyan), nitrogen (blue), silicon (yellow) and oxygen (red). The H_2O was rendered using a transparent surface (Fig. 1) to make the nano-bubbles visible.

B. Molecular simulation

Molecular dynamics (MD) was used in this work to characterize the dynamics of systems comprising CO_2 and air in pure water. All simulations were performed using NAMD 2.9[103] with the molecular constituents of the systems defined using CHARMM 22-27 (Chemistry at HARvard Molecular Mechanics) force field.[104] A list of gases and their parameters used is presented in Table 2. The TIP3P water model as optimized in CHARMM was employed.[105] The force field of amorphous silica as available in CHARMM was used.[106] The amorphous silica layers were fixed during the simulations. All molecular systems were first minimized and then equilibrated using standard procedures[107]. The depth first search method implemented in NAMD was used to

minimize the system. The systems were equilibrated using MD simulations that included constant temperature and pressure control via Langevin Dynamics (LD) and Nosé-Hoover Langevin piston pressure control. The LD temperature control, implemented in NAMD, consists of adding a random force and subtracting a friction force from each atom during simulation to keep the temperature constant. The equilibrium was considered to be achieved when the density of nano-bubbles reached a plateau. Constant pressure control was achieved with an algorithm that combines Nosé-Hoover method[108] with the control fluctuations in the barostat implemented using Langevin dynamics[109]. The velocity Verlet algorithm[110] was used for integrating the equations of motion. The cut-off distance was set to 14 Å for long range vdW interactions. A switching function of 12 Å was used to smoothly reduce the forces and energies to zero at the cut-off distance. The systems presented were investigated with periodic boundary conditions (PBC). The simulations were performed for 15 ns. The size of initial simulation box, 15.531x15.591x12.168 nm, was sufficiently large to allow the bubbles to expand without reaching the boundaries. MD simulations were run in an NPT ensemble for a total of 15 ns with a 1 fs steps after an energy minimization period of 1000 time steps. This work presents the results obtained at the temperature of 300 K and a pressure of 1.01325 atm, which corresponds to the atmospheric pressure at sea level. The smooth particle-mesh Ewald (SPME) method[111] was used to handle electro-static interactions. SPME employs B-spline function as the base function for interpolation. The use of B-spline functions reduces the number of Fast Fourier Transforms (FFTs) by half compared to the original particle-mesh Ewald (PME) method.[112] A PME tolerance of 10^{-6} was used, the PME coefficient was equal to 0.219, and a 4^{th} order interpolation was implemented. The full long-range electrostatics via SPME were evaluated every 2 fs.

B. Properties characterisation parameters

Structural descriptors of nano-bubbles were determined from the atomic density profiles of the simulated systems in the orthogonal planes (Fig. 2) at every 0.5 ns time step of the simulation. The density profiles were generated at a resolution of 1 Å using VMD. This method allows the monitoring of the dynamics of semi-principal axes *a*, *b* and *c* of nano-bubbles (Fig. 2), and their contact angle with the silica surfaces during the simulation. This was done using ImageJ. An illustration of the method involved is presented in Fig. 3. The tonalities of gray were used to automatically determine the surface of the bubbles. The two plots representing the tonalities of gray for equatorial and polar diameters that intersect in the center of the bubbles are given in Fig. 3. The contact angles between the bubbles and the silica surfaces were estimated by averaging 8 angles from two orthogonal planes of density profiles that are perpendicular to x and y axis (Fig. 2). It should be noted that up to about 2.5 ns of simulation, the bubbles did not make contact with the upper silica layer (Fig. 1), and for those cases only 4 contact angles were used. The density of gas molecules in the nano-bubbles were estimated by using three spheres of 25 Å in radius that were used to sample the space within the nano-bubbles and the local densities. These local densities were then averaged to estimate the molecular density in the nano-bubbles.

Root mean square deviation (RMSD) is used to measure the distance between a simulated structure and a starting structure. The expression of RMSD used to calculate the deviation of a molecule during MD simulation from its initial structure can be written as:

$$RMSD = \sqrt{\frac{\sum_{i=1}^{n}(r_i - r)^2}{n-1}} \tag{1}$$

where r_i refers to the position of atom *i* at time step *i; r* refers to the position of the atom *i* in the starting structure and *n* refers to the total number of atoms in the molecule. In this study, RMSD was used to assess the structural stability of N_2 and O_2 molecules and CO_2 and air nano-bubbles.

The radial distribution function (RDF) provides information on internal structure of atomic and molecular systems. In this work it is used to study the arrangement of gas molecules in the proximity of silica surface. It can be defined by the following equation:

$$g_{ij}(r) = \frac{< n_{ij}(r, r+\Delta r) >}{\rho_j 4\pi r^2 \Delta r} \quad (2)$$

where $< n_{ij}(r, r+\Delta r) >$ represents the total number of atoms of species j in a spherical shell between r and $r+\Delta r$ with the center corresponding with the center of atom i and ρ_j is the density of species j in the system. The RDF gives the probability of finding two species at the separation distance *r*.

The trajectories of gas molecules are investigated by quantifying the radial distance between the center of the nano-bubble and center of mass of the specific molecule at every simulation time step. The reference center of the nano-bubble is determined at the 15 ns time step. Gas molecules which were inside the bubbles, on their surfaces and in water at 15 ns time step were used to track their trajectory during simulation.

III. RESULTS AND DISCUSSION

Measurements of the equatorial and polar diameters during the evolution of the bubbles, summarised in Fig. 4, provided information on their expansion time and dynamics. The tri-axial parameters start from a values of *a*, *b* and *c* equal to 3 nm and evolve to average values for *a* of ~ 4 nm and for *b* and *c* of ~ 7.7 nm. It should be noted that in Fig. 4, the lines connecting the data points serve only as a guide for the eyes and do not represent the data. In Fig. 4(a) the two equatorial diameters (ED1 and ED2) (Fig. 2) and the polar diameter (PD) are presented for the CO_2 bubble over representative simulation time steps. In Fig. 4(b) the ED1, ED2 and PD are presented for the air bubble. From the figures it can be noticed that the bubbles have an expected symmetry with similar values for ED1 and ED2. The evolution of the volume of nano-bubbles is presented in Fig. 4. Based on the data, the volumetric expansion can be approximated with

a sigmoid of the form $y = a + (b-a)/(1 + exp((x-x_0)/dx))$. The fitting parameters for the volume of CO_2 bubble are a = 919524.638, b = 167085.686, x_0 = 4.33133 and dx = 2.09033 and for air bubble are a = 960632.043, b = 196634.359, x_0 = 4.955 and dx = 1.326. Fig. 4(a) and (b) indicate that the equilibrium values of the volumes of air and CO_2 bubbles are about 9.5 x 10^5 Å^3 and 9 x 10^5 Å^3 respectively. This is due to a higher solubility of CO_2 in water and its higher affinity for amorphous silica. In this study it was observed that CO_2 diffused readily in the amorphous silicon matrix. The probability of O_2 diffusing outside of the air bubble is very low in this simulation. Although the N_2 diffusion would be expected to dominate, as also indicated by this work, one would expect an increase of O_2 diffusion for a larger nano-bubble. These aspects will be further address later in this paper.

The volumetric expansion of nano-bubbles leads to a density change. The decrease in density of gas molecules and of air in the nano-bubbles is presented in Fig. 5. In this figure the lines connecting the data points provide guides for the eyes and do not represent data. The change in N_2 and O_2 density during the simulation time is shown in Fig 5(a). The average densities at equilibrium are about 0.003 a.u./Å^3 and 0.002 a.u./Å^3 for N_2 and O_2 respectively. The density for these gases, during the simulation, exhibits an exponential decay that can be described by a first order approximation: $y = a*exp(-x/t) + y_0$. The fitting parameters are a = 0.007, t = 2.639 and y_0 = 0.003 for N_2 and a = 0.006, t = 1.246 and y_0 = 0.002 for O_2. The decrease of CO_2 and air in the bubbles over simulation time indicates that they reach a similar density at equilibrium (Fig. 5 (b)). The CO_2 nano-bubble started from a higher density and reached equilibrium at about 10 ns time step. Starting from a lower density value, compared to CO_2 nano-bubble, the air bubble reached equilibrium after about 7 ns. The first order exponential decay can be used to estimate the

decrease of CO_2 and air density in the bubbles. The fitting parameters are a = 0.032 , t = 2.198 and y_0 = 0.005 for CO_2 and a = 0.012, t = 3.264 and y_0 = 0.005 for air. The results, presented later in this work, show that the density of gas equilibrates due to diffusion of gas molecules in and out the nano-bubble. This is in agreement with one of the reasons for the existence and stability of nano-bubbles explained previously by a theoretical model[113].

The analysis of contact angles results show that after about 2.5 ns, their values are relatively stable with some fluctuation within the error bar (Fig. 6). The error bar was derived from averaging over 8 data points obtained as indicated in the method section. The exception is for the first data point for which only 4 values were averaged. This case corresponds to the simulation time when the bubble was in contact only with the lower surface (Fig. 1). It should be noted that in Fig. 6 the lines do not represent data but serve as guiding aids. The average values of the contact angle at equilibrium range from 17 to 27 degrees. The variability of contact angles shown in Fig. 6 are due to nano-scopic heterogeneities and topographical diversity of the amorphous silica surface. This would be caused by any rough surface. AFM techniques indicated that amorphous silica has a roughness within about 0.3 to 0.6 nm.[114] In our study the roughness of the silica surface is about 0.35 nm.

The stability of the systems comprising of individual type of gas molecules and of air are investigated using RMSD. The results show that after about 1000 simulation states, corresponding to 5 ns, the overall systems are relatively stable (Fig. 7). O_2 exhibits a higher instability reflected in larger fluctuations in RMSD results.

The RDF was determined for O_2-Si, N_2-Si and CO_2-Si pairs (Fig. 8). The first peaks in Fig. 8 show the probability of finding the gas molecules in the first neighbouring shell of Si. The results indicate that CO_2 has the highest probability of being in the

proximity of Si followed by N_2 and O_2. One should be aware that the amplitudes of RDF are expected to be influenced by the number of molecules in the system. Visual investigations and Fig. 8 indicate that N_2 has a higher probability of being in the proximity of amorphous silica surface. The peaks evident in the RDF at about 6.5 Å for N_2-Si and CO_2-Si pairs show a relative degree of order in the system. At further distance, the order is smaller and RDF does not exhibit any peaks.

The trajectories of three representative gas molecules of CO_2, N_2 and O_2 situated inside the nano-bubbles, on their surface and in water at the end of the simulation are presented in Fig. 9, 10 and 11 respectively. Each simulation frame, which contains the coordinates of all atoms at a given time, was obtained every 5000 fs over the 15 ns simulation. Knowing that the largest tri-axial parameter has a maximum value of about 8 nm, the results presented in Fig. 9 show that the molecules move mainly within the nano-bubble. In Fig. 9(a) after about 7.5 ns (1500 simulation states) there are some evidently larger values for 2nd and 3rd molecules, with values close to 10 nm for the 3rd molecule. These indicate that CO_2 molecules can diffuse out of the nano-bubble before returning into the bubble at the end of the simulation. A similar behaviour is exhibited by the 2nd N_2 molecule (Fig. 9(b)). The 1st and 2nd of O_2 molecules have a peak at about 12.5 ns (2250 simulation state), corresponding to a diffusion process. It should be noted that the last data point corresponds with the molecule inside the nano-bubble. The results for the case when gas molecules are on the surface of the bubble exhibit also trajectories that highlight the diffusive process (Fig. 10). In Fig. 10(a) 1st molecule of CO_2 is located outside the bubble at about 2200 simulation state. The results in this figure indicate that the gas molecules are inside the nano-bubble for the majority of the time. In Fig. 10(b) all three N_2 molecules show transitory diffusion outside the air bubble. The distance from the centre of the bubble to the three O_2 molecules does not exceed 8 nm (Fig. 10(c)) which indicate no diffusion.

This is in agreement with structural investigations which revealed the presence of only one O_2 molecule outside of the air bubble at the end of the simulation. The trajectory of three distinct CO_2, O_2 and N_2 molecules situated outside the bubble at the end of simulation are presented in Fig. 11. The data for three CO_2 molecules outside the nano-bubble in Fig. 11(a) show the expected diffusion process. It can be noted for the 2nd and 3rd molecules that the value of the distance exhibits very small fluctuation for some simulation intervals. This corresponds to CO_2 molecules being in the proximity of the amorphous silica surface. In Fig. 11(b) only 1st and 3rd N_2 molecules are in the bubble during the entire simulation and close to 15 ns simulation time step. As only one O_2 molecule was identified at the end of the simulation outside the bubble, there is only one data set plotted in Fig. 11(c). Measurements of the distances between the center of the nano-bubbles and gas molecules revealed different aspects pertaining to diffusion of gas in and out of the bubbles and their dynamics.

IV. CONCLUSIONS

The present work reported from an atomistic level the expansion and stability of nano-bubbles confined by two dehydroxylated amorphous silica. The results provide the foundation for using these approaches to explore structural descriptors and dynamic characteristics of nano-bubbles. A method for precisely determining the structural parameters of nano-bubbles was introduced. The results showed the expansion of nano-bubble from a dense phase to an equilibrium phase. They indicated that this process involves a volumetric expansion and an exponential decay of gas density within the nano-bubbles. The contact angle between nano-bubbles and silica surface was found to be in the range from 17 to 27 degrees. The scattered values of contact angle were shown to be caused by heterogeneities and topographical diversity of surfaces. The results indicated

that the stability of nano-bubbles over the majority of the simulation time is due to diffusion of gas molecules in and out of the nano-bubbles. This mechanism that ensured the stability of nano-bubbles is in agreement with theoretical studies reported before. Further work could use non-equilibrium molecular dynamics to move apart the silica surface and to quantify the role of nano-bubbles on their interaction.

We thank the IBM Watson BlueGeneQ team for technical support and for generous allocation of computing resources. The constructive discussions and comments provided by Dr. Andrew Rawlinson, Dr. George Yiapanis and Dr. Matthew Downton are also acknowledged.

REFERENCES

[1] J. F. Conley, and P. M. Lenahan, Appl. Phys. Lett. **62**, 40 (1993).

[2] E. E. Stahlbush, A. H. Edwards, D. L. Griscom, and B. J. Mrstik, J. Appl. Phys. **73**, 658 (1993).

[3]A. P. Legrand, The Surface Properties of Silica, Wiley New York, (1998).

[4]R. K. Iler, The Chemistry of Silica, Wiley New York, (1979).

[5]C. R. Helms, and B. D. Deal, The Physics and Chemistry of SiO2 and the Si–SiO2 Interface, Plenum New York, (1993).

[6]R. K. Iler, The Chemistry of Silica, Wiley Interscience New York, (1979).

[7]W. Stober, A. Fink, and E. Bohn, J. Colloid Interface Sci. **26**, 62 (1968).

[8]D. L. Green, J. S. Lin, Y.-F. Lam, M. Z.-C. Hu, D. W. Schaefer, and M. T. Harris, J. Colloid Interface Sci. **266**, 346 (2003).

[9]W. Tan, W. Kemin, X. He, X. J. Zhao, T. Drake, L. Wang and R. P. Bagwe, Med. Res. Rev. **24**, 621 (2004).

[10]T. Pellegrino, S. Kudera, T. Liedl, A. J. Manoz, L. Manna and W. J. Parak, Small **1**, 48 (2005).

[11]B. A. Morrow, and I. A. Cody, J. Phys. Chem. **80**, 1995 (1976).

[12]T. A. Michalske, and B. C. Bunker, J. Appl. Phys. **56**, 2686 (1984).

[13]B. C. Bunker, D. M. Haaland, K. J. Ward, T. A. Michalske, W. L. Smith, J. S. Binkley, C. F. Melius, and C. A. Balfe, Surf. Sci. **210**, 406 (1989).

[14]L. H. Dubois, and B. R. Zegarski, J. Phys. Chem. **97**, 1665 (1993).

[15]L. H. Dubois, and B. R. Zegarski, J. Am. Chem. Soc. **115**, 1190 (1993).

[16]A. Grabbe, T. A. Michalske, and W. L. Smith, J. Phys. Chem. **99**, 4648 (1995).

[17]E. Radlein, R. Ambos, and G. H. Frischat, Fresenius J. Anal. Chem. **353**, 413 (1995).

[18]W. Raberg, and K. Wandelt, Appl. Phys. A: Mater. Sci. Process. **66**, S1143 (1998).

[19]P. K. Gupta, D. Inniss, C. R. Kurkjian, and Q. Zhong, J. Non-Cryst. Solids **262**, 200 (2000).

[20]C. A. Murray, and T. J. Greytak, Phys. Rev. B **20**, 3368 (1979); D. M. Krol, and J. G. van Lierop, J. Non-Cryst. Solids **68**, 163 (1984); L. T. Zhuravlev, Langmuir **3**, 316 (1987); B. C. Bunker, D. M. Haaland, T. A. Michalske, and W. L. Smith, Surf. Sci. **222**, 95 (1989); B. A. Morrow, and A. J. McFarlan, J. Non-Cryst. Solids **120**, 61 (1990); I. S. Chuang, D. R. Kinney, C. E. Bronnimann, R. C. Zeigler, and G. F. Maciel, J. Phys. Chem. **96**, 4027 (1992); D. R. Kinney, I.-S. Chuang, and G. F. Maciel, J. Am. Chem. Soc. **115**, 6786 (1993)

[21]M. A. Ramos, M. H. Gil, E. Schacht, G. Matthys, W. Mondelaers, and M. M. Figueiredo, Powder Technol. **99**, 79 (1998).

[22]L. Peng, W. Qisui, L. Xi, and Z. Chaocan, Colloids, and Surfaces A: Physicochem. Eng. Aspects **334**, 112 (2009).

[23]C. G. Pantano, Rev. Solid State Sci. **3**, 379 (1989).

[24]F. Kudo, and S. Nagase, J. Am. Chem. Soc. **107**, 2589 (1984).

[25]M. O'Keeffe, and G. V. Gibbs, J. Phys. Chem. **89**, 4574 (1985).

[26]D. R. Hammann, Phys. Rev. B **55**, 14784 (1997).

[27]D. Ceresoli, M. Bernasconi, S. Iarlori, M. Parrinello, and E. Tosatti, Phys. Rev. Lett. **84**, 3887 (2000).

[28]N. Lopez, M. Vitiello, F. Illas, and G. Pacchioni, J. Non-Cryst. Solids **271**, 56 (2000).

[29]M. Vitiello, N. Lopez, F. Illas, and G. Pacchioni, J. Phys. Chem. A **104**, 4674 (2000).

[30]H. Wu, D. bratko, H. W. Blach and J. H. Prausnitz, J. Chem. Phys. **111**, 7084 (1999).

[31]A. Videcoq, M. Hana, P. Abélard, C. Pagnouxa, F. Rossignola, and R. Ferrandob, Physica A **374**, 507 (2007).

[32]J. C. Chen, and A. S. Kim, Adv. Colloid Interface Sci. **112**, 159 (2004).

[33]P. Linse, Adv. Polym. Sci. **185**, 111 (2005).

[34]M. Jonsson, M. Skepo, and P. Linse, J. Phys. Chem. B **110**, 8782 (2006).

[35]A. Evilevitch, V. Lobaskin, U. Olsson, P. Linse, and P. Schurtenberger, Langmuir **17**, 1043 (2001).

[36]A. Roder, W. Kob, and K. Binder, J. Chem. Phys. 114, 7602 (2001).

[37]V. A. Bakaev, Phys. Rev. B **60**, 10723 (1999).

[38]V. A. Bakaev, and W. A. Steele, J. Chem. Phys. **111**, 9803 (1999).

[39]J. V. L. Beckers, and S. W. de Leeuw, J. Non-Cryst. Solids **261**, 87 (2000).

[40]V. I. Bogillo, L. S. Pirnach, and A. Dabrowski, Langmuir **13**, 928 (1997), V. A. Bakaev, W. A. Steele, T. I. Bakaeva, and C. G. Pantano, J. Chem. Phys. **111**, 9813 (1999); M. M. Branda, R. A. Montani, and N. J. Castellani, Surf. Sci. **446**, L89 (2000).

[41]J. Horbach, T. Stuhn, C. Mischler, W. Kob, and K. Binder, High Performance Computing in Science and Engineering 167 (2003).

[42]C. Mischler, J. Horbach, Walter Kob, and Kurt Binder, J. Phys.: Condens. Matter **17**, 4005 (2005).

[43]J. Chai, S. Liu, and X. Yang, **255**, 9078 (2009).

[44]G. Yiapanis, D. J. Henry, S. Maclaughlin, E. Evans, and I. Yarovsky , Langmuir, **28**, 17263 (2012).

[45]X. Yang, Z. Xu, and C. Zhang, J. Colloid and Interface Sci., **297**, 33 (2006).

[46]J. M. Stallons, and E. Iglesia, Chem. Eng. Sci. **56**, 4205 (2001).

[47]E. A. Leed, and C. G. Pantano, J. Non-Cryst. Solids **325**, 48 (2003).

[48]V. A. Bakaev, and W. A. Steele, J. Chem. Phys. **111**, 9803 (1999).

[49]C. D. Lorenz, M. Tsige, S. B. Rempe, M. Chandross, M. J. Stevens, and G. S. Grest, J. Comput. Theor. Nanosci. **7**, 2586 (2010).

[50]J. M. D. Lane, M. Chandross, C. D. Lorenz, M. J. Stevens, and G. S. Grest, Langmuir **24**, 5734 (2008).

[51]A. Carré, L. Berthier, J. Horbach, S. Ispas, and W. Kob, J. Chem. Phys. **127**, 114512 (2007).

[52]P. H. Poole, P. F. McMillan, and G. H. Wolf, Rev. in Mineral. **32**, 563 (1995).

[53]K. Vollmayr, W. Kob, and K. Binder, Phys. Rev. B **54**, 15808 (1996).

[54]S. N. Taraskin, and S. R. Elliott, Europhys. Lett. **39**, 37 1997; Phys. Rev. B **56**, 8605 (1997).

[55]J. Horbach, W. Kob, and K. Binder, J. Phys. Chem. B **103**, 4104 (1999).

[56]M. Benoit, S. Ispas, P. Jund, and R. Jullien, Eur. Phys. J. B **13**, 631 (2000).

[57]J. Horbach, W. Kob, and K. Binder, Eur. Phys. J. B **19**, 531 (2001).

[58]P. Scheidler, W. Kob, A. Latz, J. Horbach, and K. Binder, Phys. Rev. B **63**, 104204 (2001).

[59]A. Roder, W. Kob, and K. Binder, J. Chem. Phys. **114**, 7602 (2001).

[60]M. H. Müser, and K. Binder, Phys. Chem. Miner. **28**, 746 (2001).

[61]D. Herzbach, K. Binder, and M. H. Müser, J. Chem. Phys. **123**, 124711 (2005).

[62]A. Kerrache, V. Teboul, and A. Monteil, Chem. Phys. **321**, 69 (2006).

[63]F. Léonforte, A. Tanguy, J. P. Wittmer, and J.-L. Barrat, Phys. Rev. Lett. , **97**, 055501 (2006).

[64]Y. F. Liang, C. R. Miranda, and S. Scandolo, J. Chem. Phys. **125**, 194524 (2006); Phys. Rev. B **75**, 024205 (2007).

[65]L. Berthier, G. Biroli, J.-P. Bouchaud, W. Kob, K. Miyazaki, and D. Reichman, J. Chem. Phys. **126**, 184503 (2007); **126**, 184504 (2007).

[66]L. Berthier, Phys. Rev. Lett. **98**, 220601 (2007).

[67]E. R. Cruz-Chu, A. Aksimentiev, and K. Schulten, J. Phys. Chem. B, **110**, 21497 (2006)

[68]S. B. Trickey, S. Yip, H.-P. Cheng, K. Runge, and P. A. Deymier, J. Comput.-Aided Mater. Des. **13**, 1 (2006).

[69]H. P. Cheng, L.-L. Wang, M.-H. Du, C. Cao, Y.-X. Wan, Y. He, K. Muralidharan, G. Greenlee, and A. Kolchin, J. Comput.-Aided Mater. Des. **13**, 161 (2006).

[70]S. Joseph, and N. R. Aluru, Langmuir **22**, 9041 (2006).

[71]C. Mischler, J. Horbach, W. Kob, and K. Binder, J. Phys.: Condens. Matter **17**, 4005, (2005).

[72]J. Koplik, and J.R. Banavar, Phys. Rev. E **67,** 011502 (2003).

[73]K. Bucior, L. Yelash, and K. Binder, Phys. Rev. E **79**, 031604 (2009).

[74]S. Maruyama, T. Kurashige, S. Matsumoto, Y. Yamaguchi, and T. Kimura, Microscale Thermophys. Eng. **2**, 49 (1998).

[75]S. Maruyama, T. Kimura, and M.-C. Lu, Thermal Sci. Eng. **10**, 23 (2002).

[76]B. Shi, and V. K. Dhir, J. Chem. Phys. **130**, 034705 (2009).

[77]J. H. Saavedra, R. E. Rozas, and P. G. Toledo, J. of Colloid and Interface Science **426**, 145 (2014).

[78]D. T. Semiromi, and A. R. Azimian, Heat Mass Transfer **47**, 579 (2011).

[79]F. Leroy, and F. Müller-Plathe, J. Chem. Phys. **133**, 044110 (2010).

[80]J. R. T. Seddon, and D. Lohse, J. of Phys: Cond. Matter, 23, 133001 (2011).

[81]Y. Wang, and B. Bhushan, Soft Matter **6**, 29 (2010).

[82]V. S. J. Craig, Soft Matter **7**, 40 (2011).

[83]J. R. T. Seddon, and D. Lohse, J. Phys.: Condens. Matter **23**, 133001 (2011).

[84]J. W. G. Tyrrell, and P. Attard, Phys. Rev. Lett. **87**, 176104 (2001).

[85]P. G. de Gennes, Langmuir **18**, 3413 (2002).

[86]E.Lauga, and M. P. Brenner, Phys. Rev. E **70**, 026311 (2004).

[87]A. Maali, and B. Bhushan, J. Phys.: Condens. Matter **25**, 184003 (2013).

[88]R. Steitz, T. Gutberlet, T. Hauss, B. Klosgen, R. Krastev, S. Schemmel, A. C. Simonsen, and G. H. Findenegg, Langmuir **19**, 2409 (2003).

[89]M. Switkes, and J. W. Ruberti, Appl. Phys. Lett. **84**, 4759 (2004).

[90]A. Poynor, L. Hong, I. K. Robinson, S. Granick, Z. Zhang, and P. A. Fenter, Phys. Rev. Lett. **97**, 266101 (2006).

[91]X. H. Zhang, A. Khan, and W. A. Ducker, Phys. Rev. Lett. **98**, 136101 (2007).

[92]S. Karpitschka, E. Dietrich, J. R. T. Seddon, H. J. W. Zandvliet, D. Lohse, and H. Riegler, Phys. Rev. Lett. **109**, 066102 (2012).

[93]P. Troncoso, J. H. Saavedra, S. M. Acuña, R. Jeldres, F. Concha, and P. G. Toledo , J. Colloid Interface Sci., **424**, 56 (2014).

[94]G. Vigil, Z. Xu, S. Steinberg, and J. N. Israelachvili, J. Colloid Interface Sci. **165**, 367 (1994).

[95]V. V. Yaminsky, B. W. Ninham, and R. M. Pashley, Langmuir **14** 3223 (1998).

[96]J.-P. Chapel, Langmuir **10** 4237 (1994).

[97]L. Meagher, J. Colloid Interface Sci. **152** 293 (1992).

[98]I. U. Vakarelski, K. Ishimura, and K. Higashitani, J. Colloid Interface Sci. **227** 111 (2001); M. L. Fielden, R. A. Hayes, and J. Ralston, Phys. Chem. Chem Phys. **2** 2623 (2000).

[99]A. M. Freitas, and M. M. Sharma, J. Colloid Interface Sci. **233** 73 (2001).

[100]W. Humphrey, A. Dalke, and K. Schulten, J. Mol. Graph. **14**, 33 (1996).

[101]C. A. Schneider, W. S. Rasband, and K. W. Eliceiri, Nature Methods **9**, 671 (2012).

[102]C. R. Woese, Proc. Natl. Acad. Sci. **54**, 71 (1965).

[103]J. C. Phillips, R. Braun, W. Wang, J. Gumbart, E. Tajkhorshid, E. Villa, C. Chipot, R. D. Skeel, L. Kale, and K. Schulten, J. Comput. Chem. **26**, 1781 (2005).

[104]A. D. MacKerell, D. Bashford, M. Bellott, R. L. Dunbrack, J. D. Evanseck, M. J. Field, S. Fischer, J. Gao, H. Guo, S. Ha, D. Joseph-McCarthy, L. Kuchnir, K. Kuczera, F. T. K. Lau, C. Mattos, S. Michnick, T. Ngo, D. T. Nguyen, B. Prodhom, W. E. Reiher, B. Roux, M. Schlenkrich, J. C. Smith, R. Stote, J. Straub, M. Watanabe, J. Wiorkiewicz-Kuczera,

D. Yin, and M. Karplus, J. Phys. Chem. B **102**, 3586 (1998); N. Foloppe, and A. D. MacKerell, J. Comput. Chem. **21**, 86 (2000).

[105]W. L. Jorgensen, J. Am. Chem. Soc. **103**, 335 (1981).

[106]E. R. Cruz-Chu, A. Aksimentiev, and K. Schulten, J. Phys. Chem. **110**, 21497 (2006).

[107]A. Bojovschi, M. S. Liu, and R. J. Sadus, J. Chem. Phys. **137**, 075101 (2012); **140**, 115102 (2014).[106]

[108]G. J. Martyna, D. J. Tobias, and M. L. Klein, J. Chem. Phys **101**, 5 (1994).

[109]S. E. Feller, Y. Zhang, R. W. Pastor, and B. R. Brooks, J. Chem. Phys. **103**, 11 (1995).

[110]W. C. Swope, H. C. Andersen, P. H. Berens, and W. K. R., J. Chem. Phys. **76,** 637 (1982).

[111]U. Essmann, L. Perera, M. L. Berkowitz, T. Darden, H. Lee, and L. G. Pedersen, J. Chem. Phys. **103**, 8577 (1995).

[112]W. Humphrey, A. Dalke, and K. Schulten, J. Mol. Graphics **14**, 33 (1996).

[113]J. H. Weijs, and D. Lohse, Phys. Rev. Lett, **110**, 054501, (2013).

Table I. Summary of gases in pure water carried out in this work at 300K using an integration time step of 1fs.

System	Number of atoms	Number of N2	Number of O2	Number of CO2
SiO_2, CO_2 and H_2O	248927	-	-	489
SiO_2, O_2, N_2 and H_2O	248180	288	72	-

Table II. CHARMM parameters for N_2, O_2 and CO_2 used in this work.

	Specific charge	Bond length (Å)	Bond constant (kcal/mole/A^2)	σ(Å)	ε(kcal/mol)
CO2					
C	0.6			-0.06	1.56
CO1	-0.3			1.69	-0.17
CO2	-0.3			1.69	-0.17
C-CO1		1.16	937.96		
N2					
N	0			1.65	-0.2
N	0			1.65	-0.2
N-N		1.1	1007		
O2					
O	0			1.77	-0.15
O	0			1.77	-0.15
O-O		1.28	1180		

Figures

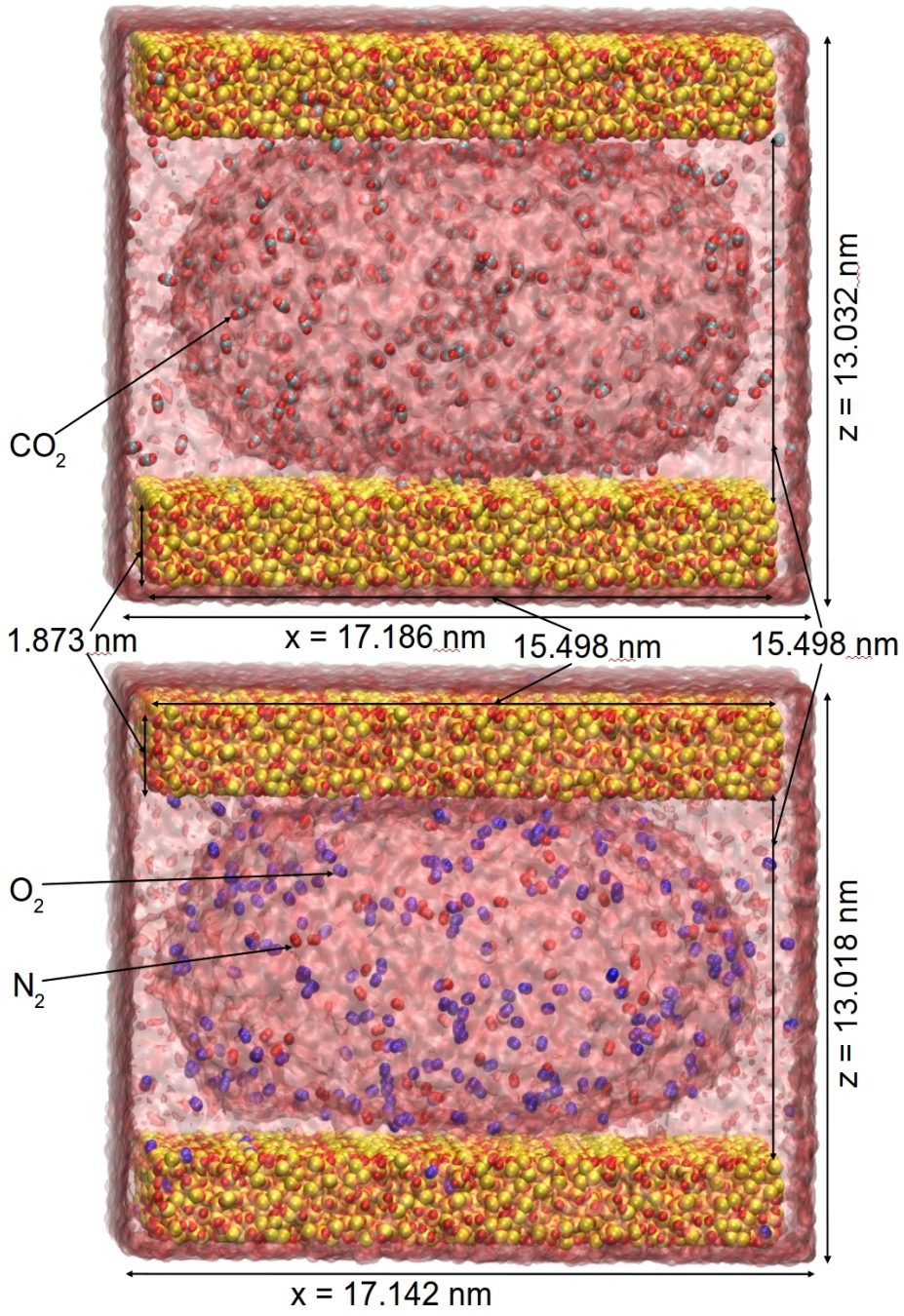

FIG. 1. The simulation systems at 15 ns. The systems consist of CO_2 and air bubble (N_2 and O_2) between two identical layers of amorphous silica immersed in water. The gas molecules and the silica layer are represented using van der Waals spheres. The water is rendered using a transparent surface. The y dimension is 17.170 nm for the system with air and 17.143 nm for the system with CO_2.

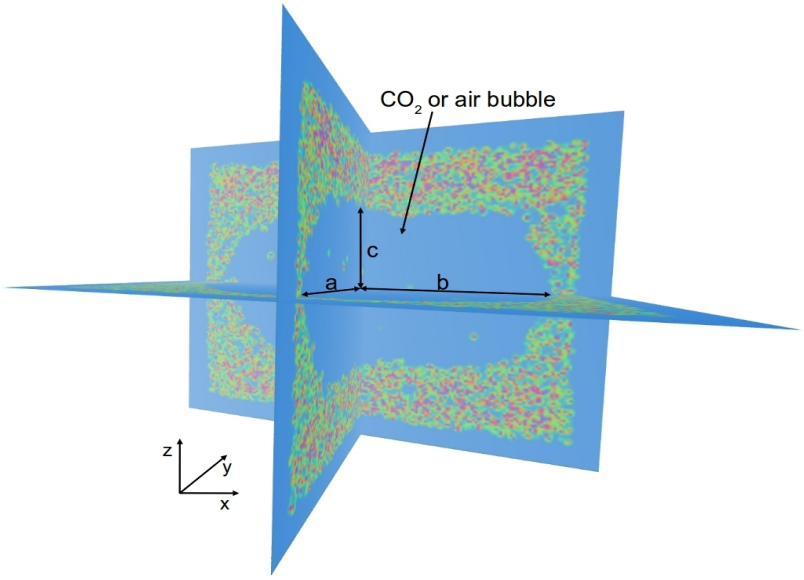

FIG. 2. Atomic density profiles of the orthogonal planes intersecting in the center of the gas bubble. The semi-principal axes *a*, *b* and *c* of the tri-axial ellipsoid used to approximate the bubbles. The blue areas represent empty space while the other color zones indicate the presence of atoms. The descending atomic density is represented by colours that starts from dark red followed by orange, yellow, green and ends at blue. The details are resolved at 1 Å resolution.

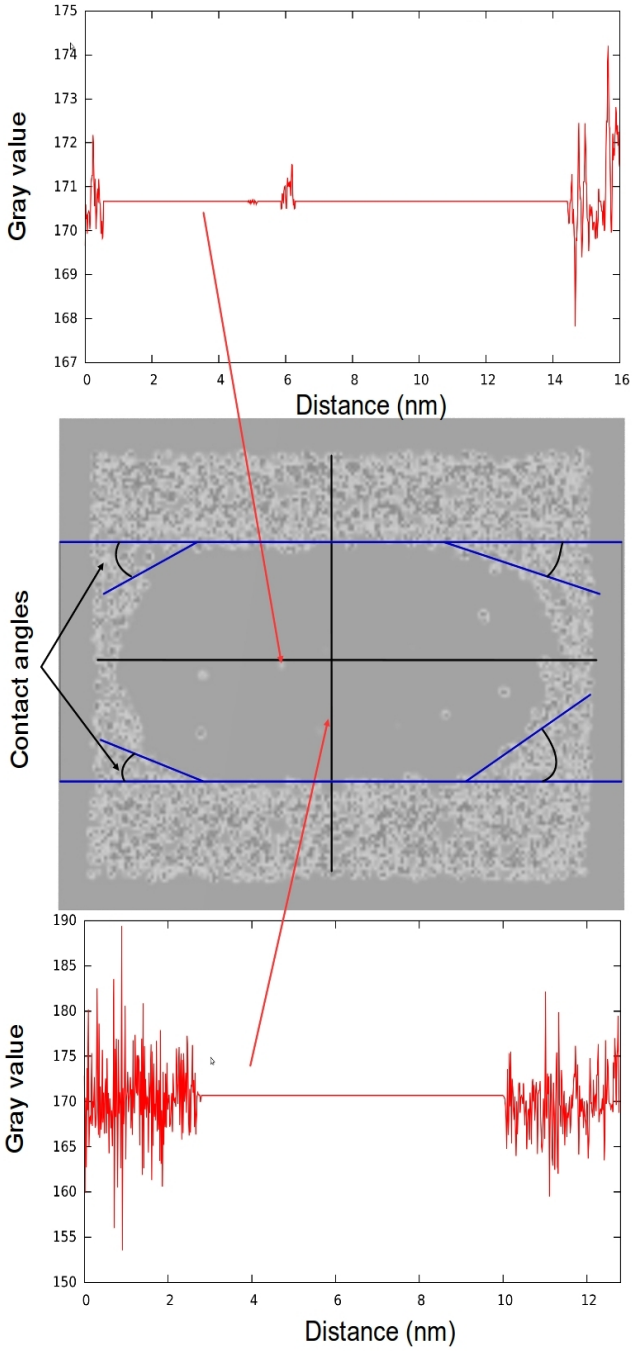

FIG. 3. Illustrative method used to estimate the equatorial and polar diameters and the contact angle. The image processing performed using ImageJ allows identifying precisely where the atom density changes via the tonality of the gray scale. This allows determining the equatorial and polar diameters. The ability to quantify the contact angles is also facilitated by ImageJ package.

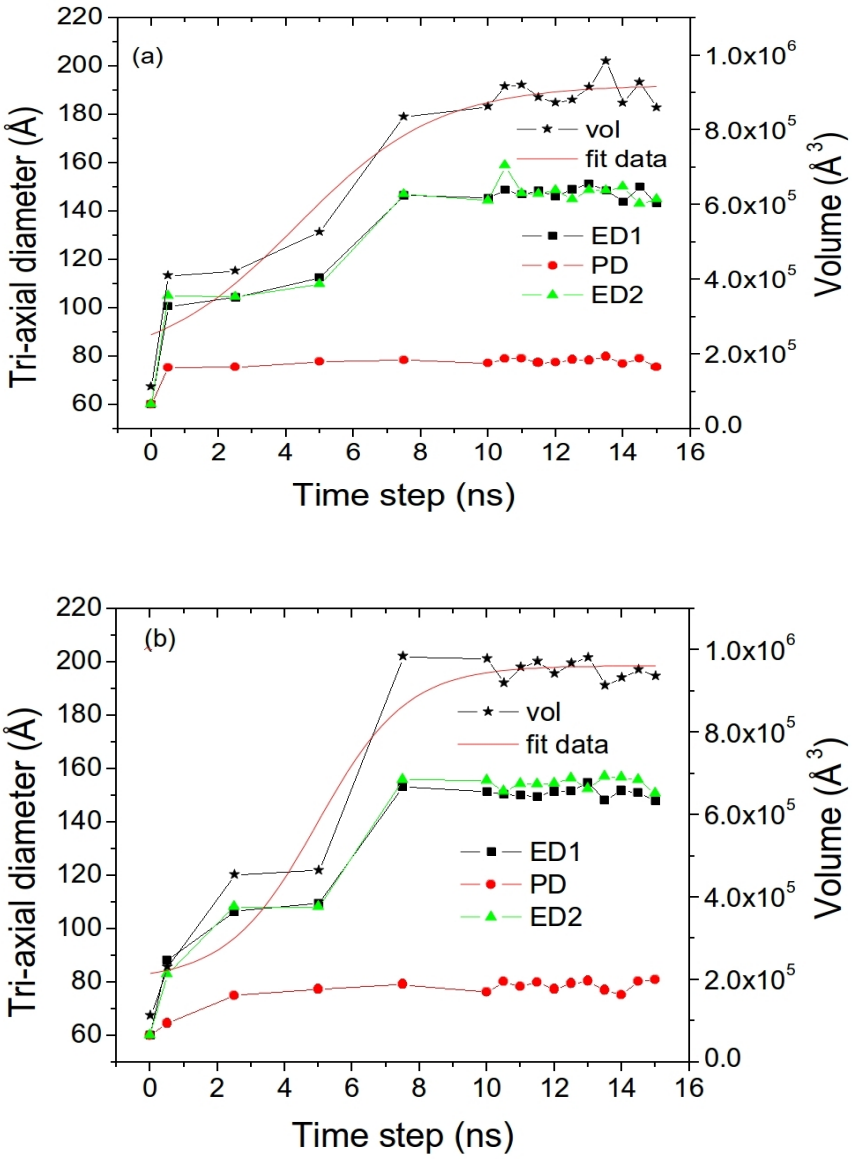

FIG. 4. Geometrical descriptors of the bubbles. These include the equatorial diameters (ED1 and ED2), polar diameter (PD) and the volume (vol) of the tri-axial ellipsoid used to approximate the air (a) and CO_2 (b) bubbles. The volumetric expansion of CO2 and air bubbles over the simulation can be approximated by a sigmoid (fit data).

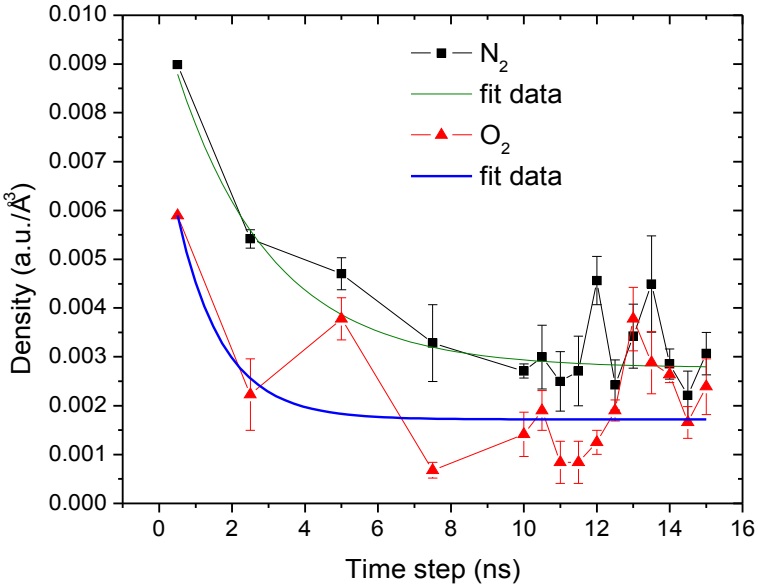

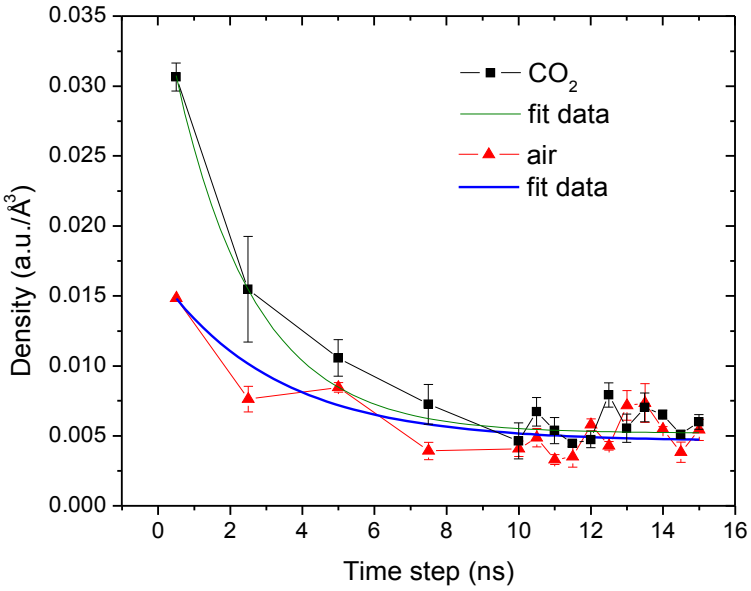

FIG. 5. The density of gases in the nano-bubbles. The data is averaged from three values obtained in three regions of the bubbles that sample the nano-bubble volume. The regions were defined by spheres of radius equal to 2.5 nm. The individual density of N_2 and O_2 in the air bubble are shown in (a) while the density of CO_2 and air bubbles are presented in (b). The densities over the simulation time follow a first order exponential decay (fit data).

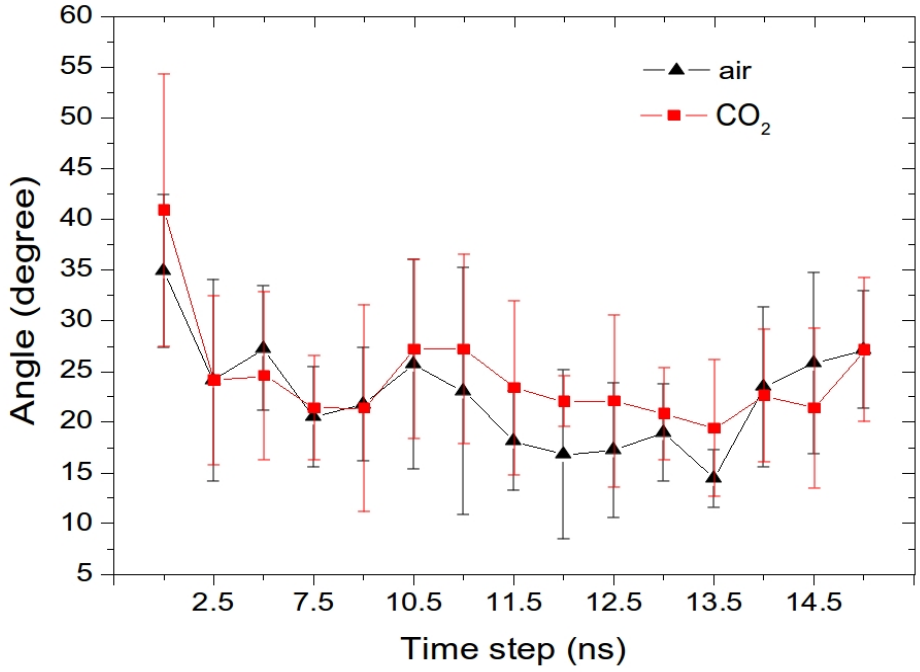

FIG. 6. Contact angle between the air and CO_2 nano-bubbles and the amorphous silica surface. Eight values were collected to average the contact angle at each time step. The values of the contact angle were obtained using the method presented in Figure 3 whereby two orthogonal planes, perpendicular on x and y axis (Figure 2), of atom density profiles were used.

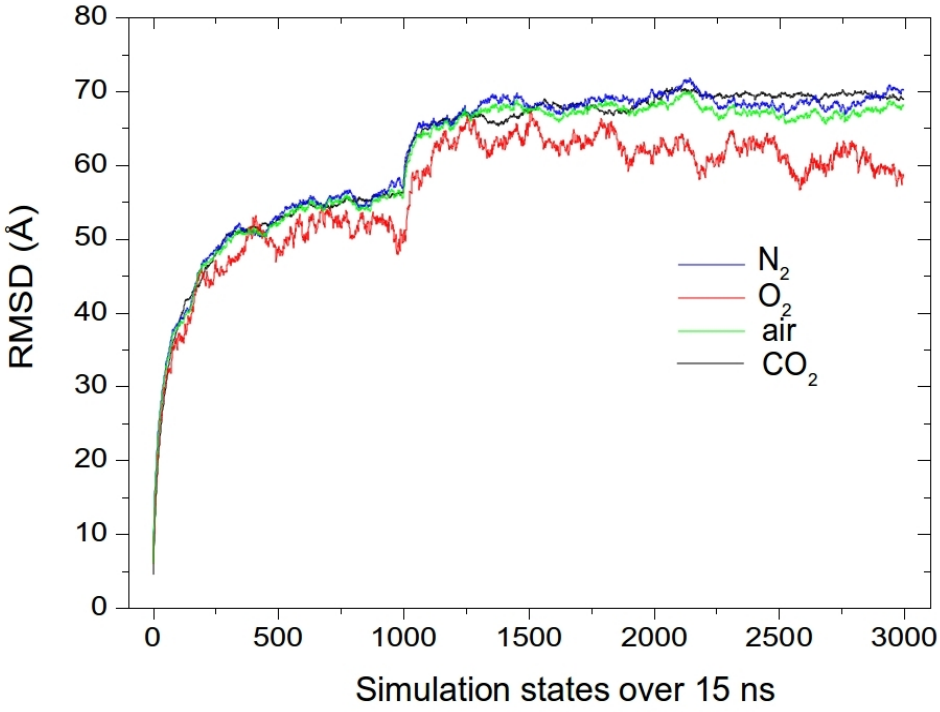

FIG. 7. The RMSD of the individual sets of gas molecule: N_2, O_2 and CO_2 and of air over the time of simulation.

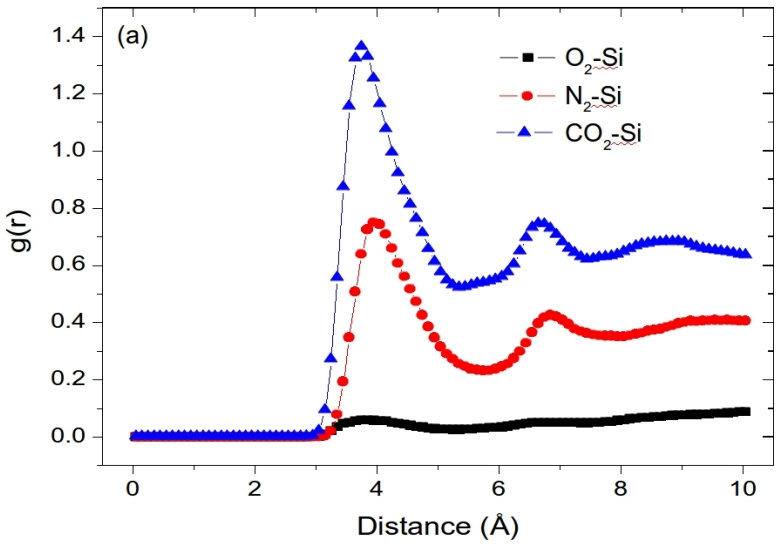

FIG. 8. The RDFs for O_2-Si, N_2-Si and CO_2-Si obtained from the last 12.5 ns of the simulated systems.

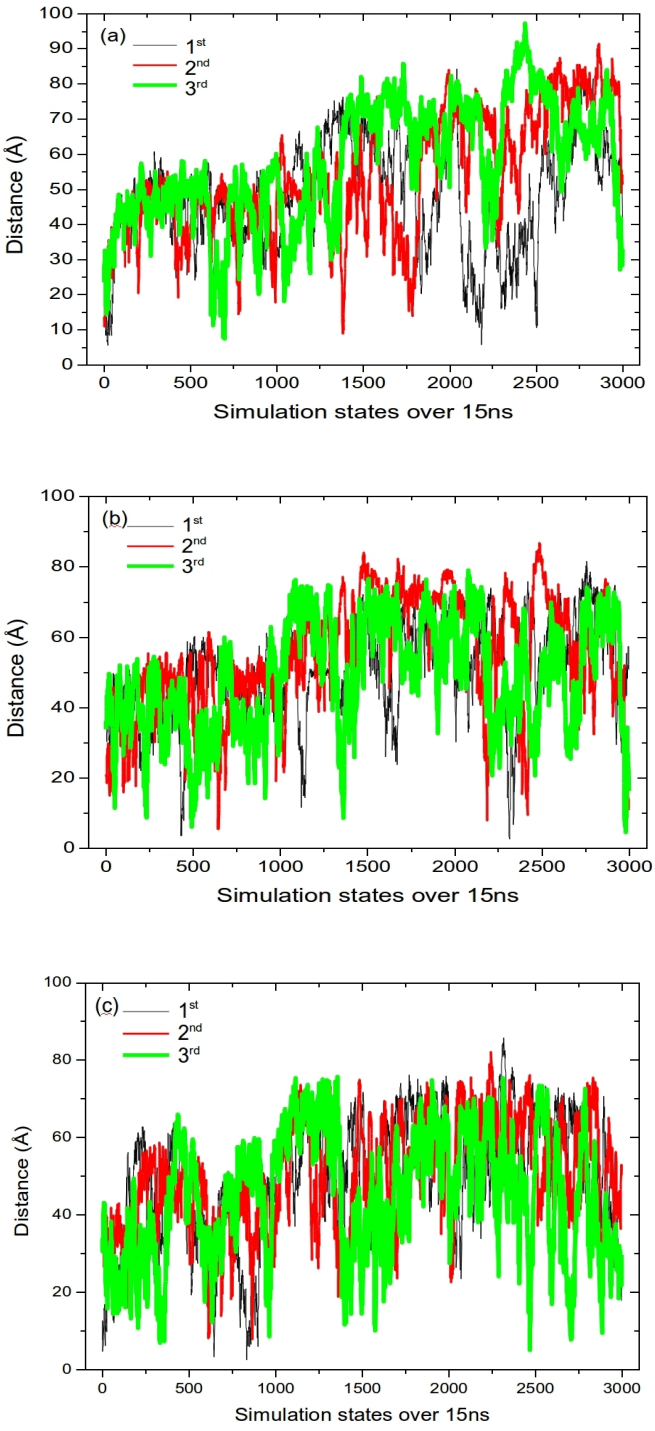

FIG. 9. Representative dynamic displacement of CO_2 (a), N_2 (b) and O_2 (c) gas molecules, situated inside the bubbles at the end of the simulations. The displacement was computed with reference to the centre of the bubbles estimated at 15 ns time step. The three data sets in each plot (1^{st}, 2^{nd} and 3^{rd}) correspond to three distinct gas molecules.

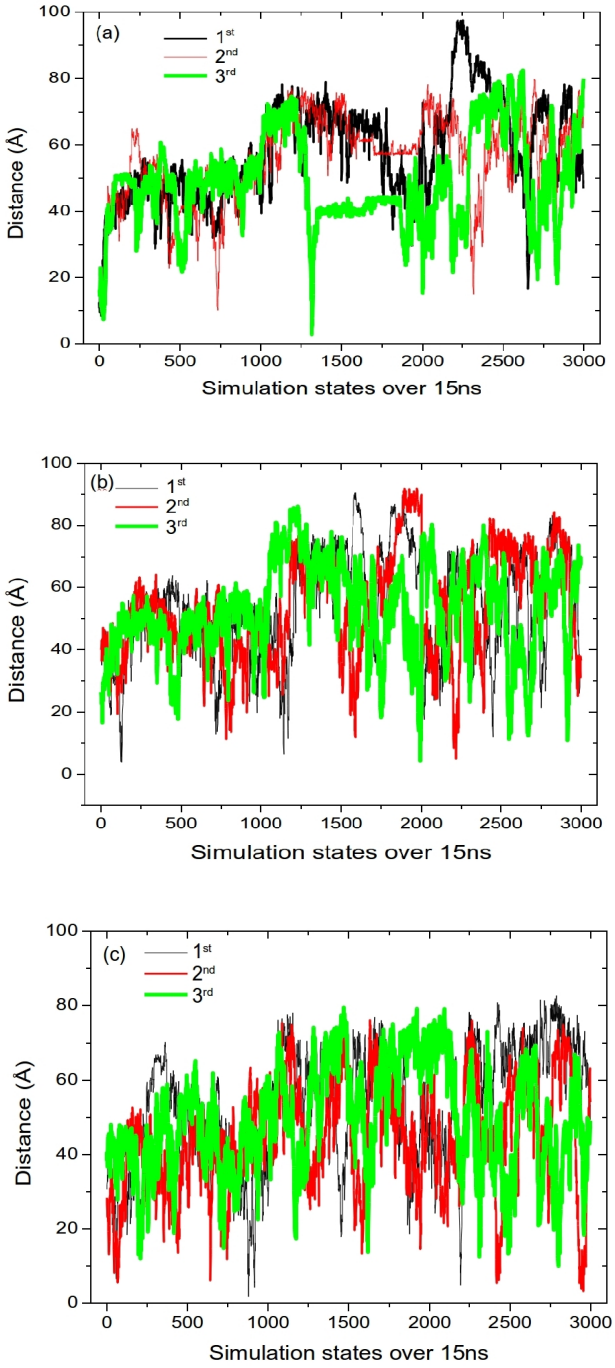

FIG. 10. Representative dynamic displacement of CO_2 (a), N_2 (b) and O_2 (c) gas molecules, situated on the surface of the bubbles at the end of the simulations. The displacement was computed with reference to the centre of the bubbles estimated at 15 ns time step. The three data sets in each plot (1^{st}, 2^{nd} and 3^{rd}) correspond to three distinct gas molecules.

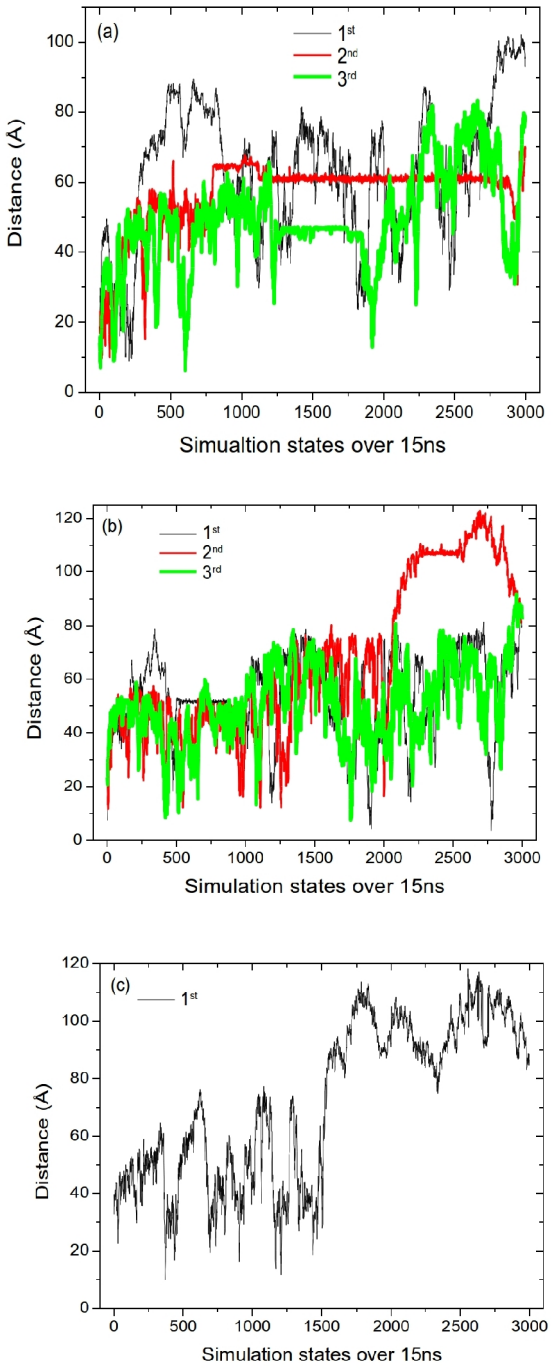

FIG. 11. Representative dynamic displacement of CO_2 (a), N_2 (b) and O_2 (c) gas molecules, situated in water, outside of the bubbles at the end of the simulations. The displacement was computed with reference to the centre of the bubbles estimated at 15 ns time step. The three data sets in each plot (1^{st}, 2^{nd} and 3^{rd}) correspond to three distinct gas molecules. Only one O2 molecule was identified outside the bubble after 15 ns (c).